Fluorescent silica MCM-41 nanoparticles based on flavonoids: Direct post-doping encapsulation and spectral characterization

Anton Landström, Silvia Leccese, Hagop Abadian, Jean-François Lambert, Isabella Concina, Stefano Protti, Ari Paavo Seitsonen, Alberto Mezzetti

▶ **To cite this version:**

Anton Landström, Silvia Leccese, Hagop Abadian, Jean-François Lambert, Isabella Concina, et al.. Fluorescent silica MCM-41 nanoparticles based on flavonoids: Direct post-doping encapsulation and spectral characterization. Dyes and Pigments, 2021, 185, pp.108870 -. 10.1016/j.dyepig.2020.108870 . hal-03493406

HAL Id: hal-03493406
https://hal.science/hal-03493406v1

Submitted on 17 Oct 2022

HAL is a multi-disciplinary open access archive for the deposit and dissemination of scientific research documents, whether they are published or not. The documents may come from teaching and research institutions in France or abroad, or from public or private research centers.

L'archive ouverte pluridisciplinaire **HAL**, est destinée au dépôt et à la diffusion de documents scientifiques de niveau recherche, publiés ou non, émanant des établissements d'enseignement et de recherche français ou étrangers, des laboratoires publics ou privés.

Distributed under a Creative Commons Attribution - NonCommercial 4.0 International License

Version of Record: https://www.sciencedirect.com/science/article/pii/S0143720820315679
Manuscript_aed0dea55bf71deef780d169373e5e4a

Fluorescent silica MCM-41 nanoparticles based on flavonoids: direct post-doping encapsulation and spectral characterization

Anton Landström[1], Silvia Leccese[2], Hagop Abadian[2], Jean-François Lambert[2], Isabella Concina[1], Stefano Protti[3], Ari Paavo Seitsonen[4,5], Alberto Mezzetti[2,*]

[1] Division of Materials Science, Department of Engineering Sciences and Mathematics, Luleå Tekniska Universitet, Luleå, SE-971 87 Sweden

[2] Laboratoire de Réactivité de Surface UMR CNRS 7197, Sorbonne Université, 4 place Jussieu, F-75005 Paris, France

[3] PhotoGreen Lab, Department of Chemistry, University of Pavia, Viale Taramelli 10, I-27100, Pavia, Italy

[4] Département de Chimie, Ecole Normale Supérieure, 24 rue Lhomond, F-75005, Paris, France

[5] Paris Sciences et Lettres Université, Sorbonne Université et Centre National du Recherche Scientifique (CNRS), F-75005, Paris, France

*corresponding author : alberto.mezzetti@sorbonne-universite.fr

Abstract

Flavones and flavonols are naturally-occurring organic molecules with interesting biological, chemical and photophysical properties. In recent years their interaction with silica surfaces has received increasing attention. In this work, the flavonol 3-hydroxyflavone (3HF) and the flavone 7-hydroxyflavone (7HF) have been encapsulated in MCM-41 mesoporous silica nanoparticles (NP) *via* a post-doping procedure, and their photophysics characterized by both steady state and time-resolved spectroscopic techniques. Both flavonoid-doped NPs resulted to be highly fluorescent, even after two months of exposure to air at room temperature. UV light irradiation results in a moderate decrease of the fluorescence quantum yield. Complementary UV-Vis and fluorescence experiments of 3HF and 7HF in solutions and TD-DFT calculations to simulate absorption and emission spectra have been carried out in order to better rationalize the exact nature of the emitting species. Whereas for 3HF-doped NPs the tautomer emission in the green predominates, the fluorescence of 7HF-doped NPs is likely to arise from the cationic or the phototautomeric form of the flavonoid. The results show that organic fluorophore-based fluorescent silica NPs can be easily obtained by a post-doping procedure and represent a first step towards the development of a simple strategy for the encapsulation in MCM-41 NPs of flavonoids and other organic molecules.

© 2020 published by Elsevier. This manuscript is made available under the CC BY NC user license
https://creativecommons.org/licenses/by-nc/4.0/

Introduction

The flavonoid moiety, that consists of two aromatic rings (A, B in Fig. 1a) connected by a pyrane core C, is largely diffuse in the vegetal kingdom. Most molecules belonging to this class play a key role in plants, as photoprotective agents [1] and antioxidants [2] as well as in plant physiology [3]. Furthermore, flavonoids exhibit interesting biological properties [4, 5], including, among others, antioxidant [6-9], neuroprotective [10-12] and anti-cancer activity [13-15]. Flavonoids have also found wide application in analytical chemistry [16, 17].

3-hydroxyflavone (3HF) and 7-hydroxyflavone (7HF) are widely studied (often in parallel) as they possess a hydroxyl group in a key position [18-21]. Furthermore, both 3HF and 7HF have interesting biological [22-24], chemical [9, 21] and photochemical properties [25, 26 and refs therein].

Their photophysical behaviour is of particular interest. Both molecules are fluorescent [25,26], showing strong environment-dependent emission properties, but whereas 3HF has been widely studied and characterized in detail [26 and refs. therein], the photophysics of 7HF has been rationalized only a few years ago [25].

In 3HF, absorption of UV light from the ground state N leads to the singlet N* ($h\nu_1$) excited state. This excitation is followed by the excited-state intramolecular proton transfer (ESIPT) from the 3-OH to the C=O group to give to the tautomeric excited form T*, which emits in the 500-540 nm region ($h\nu_T$), showing a remarkable Stokes shift value. However, in polar or protic media, the ESIPT process is hampered due to specific 3HF-solvent interactions, so that fluorescence from the N* state ($h\nu_N$) can take place competitively. As a result, in these media a dual fluorescence is normally observed [26]. This is the main reason for the widespread use of 3HF (and of its derivatives) as fluorescent probes in several fields (see [27, 28] for reviews): the ratio between the intensity of the N* and T* bands - as well as parameters such as, among the others, the bandwidth, fluorescence lifetimes and the exact position of emission bands- strictly depends on the microenvironment.

3HF-based sensors for the detection and monitoring of several analytes have also been developed (see for instance [28-31] and references therein). In addition, the molecular environment around 3HF (solvents, but also protein binding pockets, nanocavities, etc) can also induce a partial, ground state deprotonation of the 3-OH group, leading to the formation of an anionic species with completely different photophysics [26, 27, 32]. The anion absorbs at higher wavelength than the neutral form and emits ($h\nu_2$ and $h\nu_A$ in Figure 1, respectively) in the 460-490 nm region, half-way between the two emission peaks of the dual fluorescence (which becomes therefore a triple fluorescence). As an example, for 3HF in methanol (MeOH) N* emits at 406 nm, T* at 528 nm, and A* at 481 nm [26].

7HF has a different photophysics [25], since direct ESIPT cannot take place. The molecule can exist as neutral N, anion A, and cation C, depending on the basic/acid properties of the surrounding

microenvironment, while four excited state forms can exist, namely neutral N*, cation C*, anion A*, and phototautomer T*. A* can be formed either by direct excitation of the ground-state anion, or by photodissociation of the N* form; the T* formation depends on the acidity of the environment and can be formed by C* photodissociation or via photoinduced protonation of A* (see Figure 1). Despite the different species involved in its photophysics, 7HF emission has so far found much less applications than 3HF (see for instance [33]).

The interaction between flavonoids and silica matrices is an active research topic interesting several fields, ranging from optics [34, 35 and refs therein] to analytical chemistry (see for instance [36, 37]). Among the different applications, one should mention the development of silica nanoparticles (NPs) for flavonoid delivery [38, 39] or with special characteristics given by the flavonoids, such as antioxidant [40, 41] or fluorescent properties [42, 43].

MCM-41 silica NPs are particularly interesting matrices and their relevance goes even beyond the already mentioned fields, as they are used for in chromatography of flavonoids [44], solid-state extraction of flavonoids [45] and encapsulation of flavonoids for their preservation [40, 46, 47]. However, a better understanding of the interaction of flavonoids with the silica surface of MCM-41 nanopores is actually lacking.

In the present article we describe a simple procedure for the encapsulation of 3HF and 7HF in MCM-41 silica NPs and the detailed characterization of the so-prepared materials, with a special emphasis on their emission properties. A series of parallel experiments were carried out on isolated flavonoids in solution under specific conditions, in order to rationalize the nature of the emitting species. Besides their obvious relevance for their possible application in fluorescence, the particular environment-sensitive photophysics of the two monohydroxyflavones can also provide information on the interactions of the two molecules with the silica surface in MCM-41 NPs.

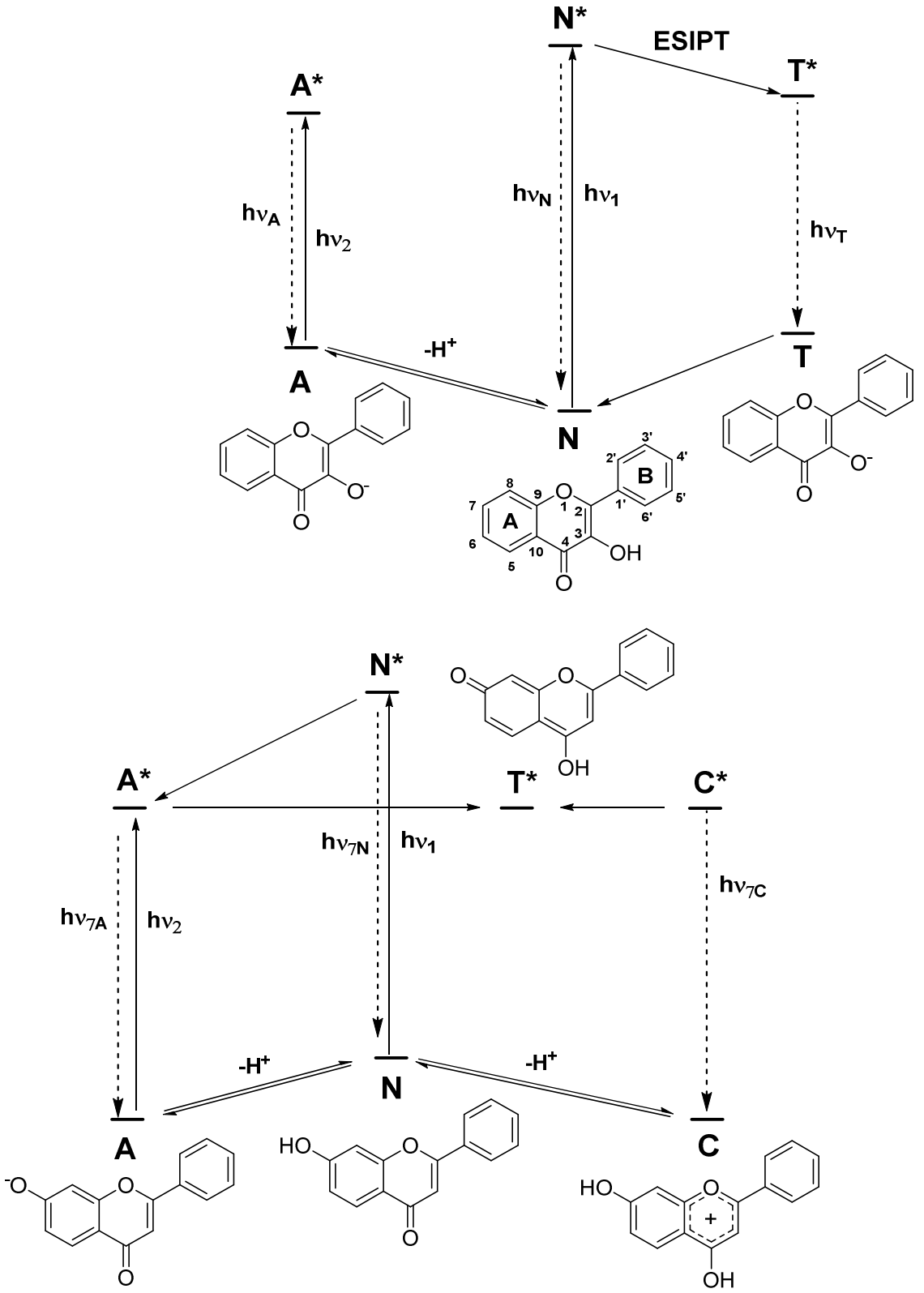

Figure 1. Upper panel: Photophysics of 3-hydroxyflavone (3HF). ESIPT : Excited State Intramolecular Proton Transfer. The numbering scheme of flavonoids is also shown. Lower panel: Photophysics of 7-hydroxyflavone (7HF), according to Ref. [25].

Materials and methods

Chemicals. 3-HF and 7-HF were purchased from Sigma-Aldrich and recrystallized from cyclohexane. Acetonitrile (MeCN) for post-doping procedure was of spectroscopic grade; for fluorescence analysis anhydrous acetonitrile was employed.

Synthesis of silica NPs. MCM-41 NPs were prepared by following the protocol described by Meynen et al. [48]. An aqueous solution of cetyltrimethylammonium bromide (CTAB), mixed with aqueous ammonia was left under stirring at a constant temperature of 35°C. Then tetraethyl orthosilicate (TEOS) was added. The TEOS/CTAB/NH_4OH mixture was left at the same temperature for 2 hours; afterwards, the system was transferred to a tightly sealed Teflon bottle placed in a drying oven at100°C and left under autogenous pressure overnight. After filtration, the final step was the removal of CTAB within the pores of the MCM-41 by calcination. The calcination process was the following: the solid sample was placed in a crucible in a programmable calcination oven under ambient air and the temperature was increased from 20°C to 300°C in 2 ½ hours. Then the temperature was kept constant at 300°C for 2 hours. Subsequently, temperature was increased from 300 to 550°C in 2 hours. Then the temperature was kept constant at 550°C for 12 hours. This liberated the mesoporous space of the MCM-41 silica material.

Nitrogen physisorption (see Figure 2) was performed on the solid material at 77K. The BET analysis showed a high surface area for the MCM-41 around 885m^2/g. The pore size distribution was determined using BJH (Barrett–Joyner–Halenda) treatment, resulting in a sharp peak for a pore size of 2.62 nm. The porous volume was 0.8002 cm^3/g.

Preparation of flavonoid-doped NPs MCM-41 NPs were added to MeCN solutions of 3HF and 7HF. Samples were stirred for 5 minutes, centrifuged for 45 minutes at 4000 rpm in order to separate the solid (containing MCM-41 matrix with the flavonoids encapsulated). The precipitate was left exposed to air for 48h in a Petri dish to let the MeCN evaporate.

Characterization of flavonoid-doped NPs X-ray diffraction (XRD) patterns of the samples were recorded with a Bruker D8 Advance powder diffractometer, using Cu Kα radiation generated at 40 kV and 40 mA and equipped with an X′Celerator detector.

Fourier Transform Infrared (FTIR) experiments were performed on a Bruker Vertex 80 rapid-scan spectrometer in the transmission mode equipped with a MCT detector. Samples were sandwiched between two CaF_2 disks and sealed with parafilm.

UV-Vis spectra of flavonoids in silica NPs were recorded with an Agilent Cary5000 spectrophotometer. An integrating sphere was used to record reflectance; spectra were obtained through Kubelka-Munk transform.

Steady-state photoluminescence spectra of flavonoids in silica NPs were recorded with Edinburgh instruments FLS980 spectrofluorimeter. A Xenon arc lamp was used as excitation source. Quantum yield

was determined by measuring scattering/absorption and emission in an integrating sphere. Photobleaching tests were performed by doing repeated emission scans of the samples on silica in 3-minute intervals.

Time-resolved photoluminescence spectra of flavonoids in silica NPs were recorded with Edinburgh instruments LS980 spectrofluorimeter. A 372 nm picosecond pulsed diode laser was used as excitation source. The lifetime was determined by deconvoluting the measured data and the instrument response function, then fitting the data with a multi-exponential function. The relative number of photons from each decay path is indicated in the plots.

UV-Vis absorption spectra in MeCN solutions were carried out by means of a Jasco V-550 spectrophotometer or by a Agilent Cary 5000 spectrophotometer. Fluorescence spectra of MeCN solution were carried out on a Perkin Elmer LS-55 spectrofluorometer or on a Edinburgh instruments FLS980 spectrofluorimeter.

Theoretical calculations. Density functional theory (DFT) [49] and time-dependent DFT [50] calculations were performed on both flavonoids in different states (neutral, tautomer, anion, cation). DFT was used to calculate the ground-state S_0 geometries and vibrational spectra; TD-DFT for the photon absorption and fluorescence spectra, the latter in the first singlet state S_1. We employed the B3LYP [51] as the approximation in the exchange-correlation functional. The basis set cc-pVTZ in the calculation of the vibrational spectra and aug-cc-pVTZ in the calculations of TDDFT were used unless otherwise mentioned. The calculations have been performed with a free-standing molecule and using implicit solvation within the conductor-like polarisable continuum model (CPCM) [52] for acetonitrile.
The computer codes ORCA [53] and Gaussian09 Revision A.02 [54] were used. We applied large integration grids and strict convergence criteria, "Grid5" and "$a" in the input of ORCA and "Integral(UltraFine)" in the input of G09.

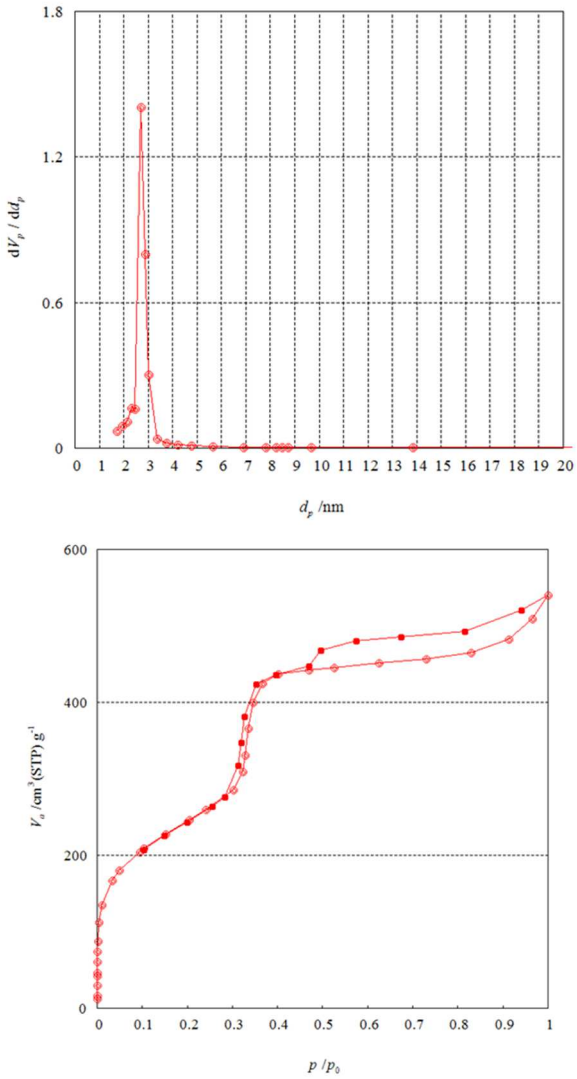

Figure 2. BJH pore distribution (upper panel) and full N_2 physisorption isotherm (lower panel)

Results and discussion

UV-vis spectra of MCM-41 NPs fabricated by impregnation of the bare MCM-41 NPs in 10^{-3} M solutions of 3HF and 7HF in MeCN and subsequent solvent evaporation are shown in Fig. 3. The spectra confirm that 3HF and 7HF have been successfully encapsulated in the silica NPs.

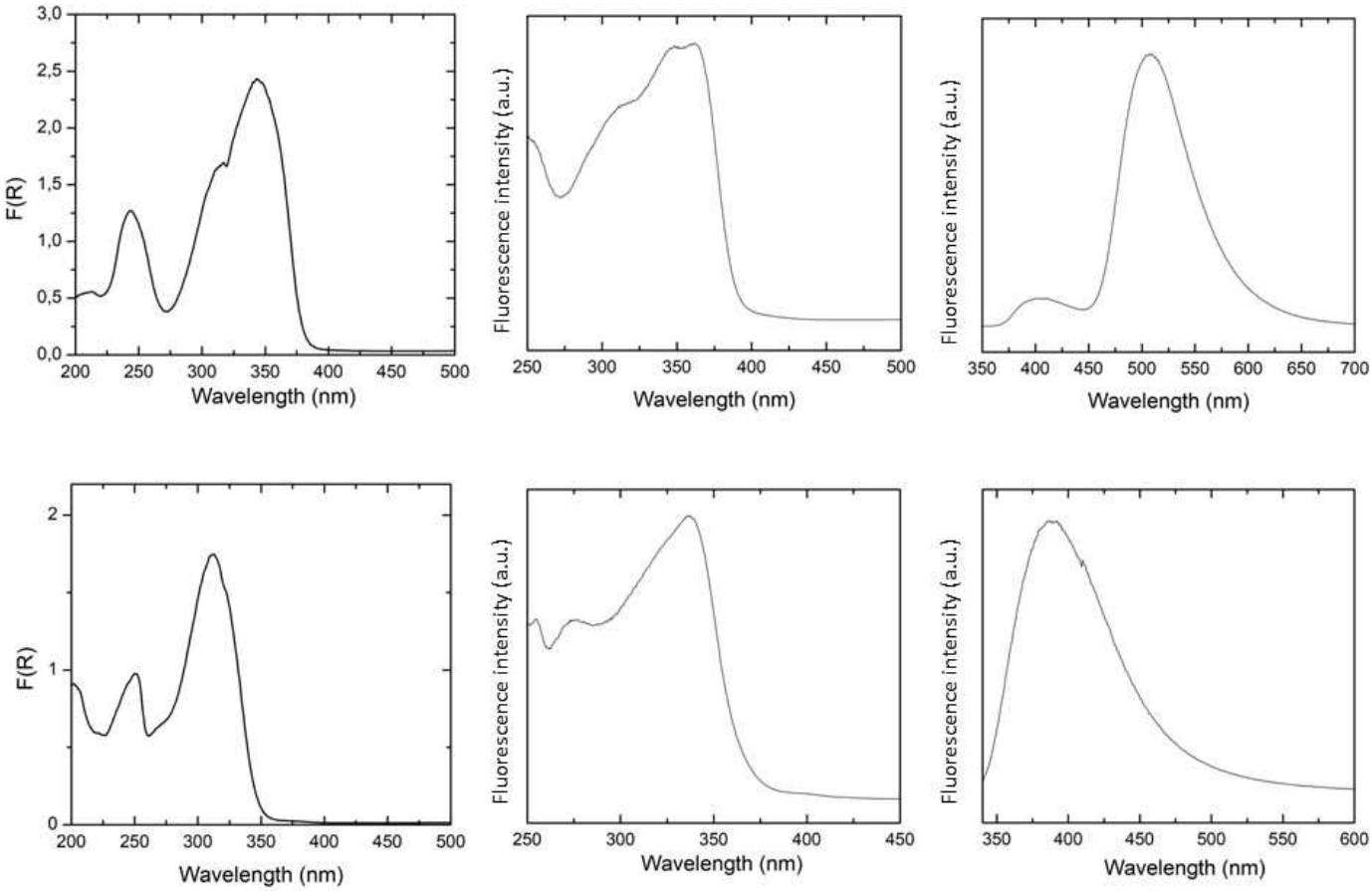

Figure 3. UV-Vis, fluorescence excitation spectra, and emission spectra of 3HF-doped MCM-41 NPs (upper traces) and of 7HF-doped MCM-41 NPs (lower traces). For a detailed description see also Table 1 and 2.

It was not however possible to precisely quantify the amount of flavonoid encapsulated (normally carried out by looking at the variation of the absorbance of the solution before and after the impregnation) because of turbidity problems, as some MCM-41 was remaining as a suspension. Interestingly, when carrying out the procedure with much more diluted 10^{-5} M solutions (not shown), the absorbance of the solution after the withdrawal of flavonoids by MCM-41 impregnation was just divided - roughly - by a factor of two. This suggests that there are some sites with a rather strong affinity (strongly negative free enthalpy of adsorption) of the silica for the two flavonoids, since adsorption is already significant at a low equilibrium concentration.

XRD results clearly indicate that no formation of 3HF or 7HF microcrystals occurs (see Figures S1 and S2 in ESI). This suggests that 3HF and 7HF are molecularly adsorbed on the surface and thus, that the maximum adsorption capacity of the NP is not reached. The low intensity of characteristic IR peaks (see later) confirms that only a limited amount of flavonoid is adsorbed.

FTIR spectra of flavonoid-loaded NPs (see Figure S3 in ESI) shows that MeCN is partially retained within the structure in both cases (peaks at 1375, 1421, 1443, 2294-8 cm^{-1}); however, the interaction of MeCN molecules with the surface seems to be different in the presence of 3HF and 7HF (see the band at 2253 cm^{-1} that is present in 7HF-loaded NPs but absent in 3HF-loaded NPs, and the band at 2263 cm^{-1} that is very intense in 3HF-loaded NPs but visible as a weak shoulder in 7HF-loaded NPs, Figure S3). It should be noticed that FTIR spectra show very low intensity bands arising from the two flavonoids (see band at 1483 cm^{-1} for 3HF [55]; band at 1646 cm^{-1} for 7HF [56]), suggesting a low loading in both cases. This is not surprising, given the hydrophilic character of the silica surface and the rather hydrophobic character of the two flavonoids. It should be pointed out however that IR bands from the silica matrix, from adsorbed water and MeCN probably hide other IR flavonoid bands (for instance the relatively intense band of 3HF expected at ~1620 cm^{-1} [57] which is not distinguishable in our FTIR spectrum).

UV-Vis spectra clearly show that inside the silica matrix the main absorbance properties of the flavonoids remain unaltered compared to those observed in solution, suggesting that in the majority of 3HF and 7HF molecules no chemical modification is taking place because of the interaction of the silica matrix. However, some significant shifts are observed for the main UV absorption band. All the main bands see their amplitude strongly diminished after 10 minutes of strong UV illumination in all samples, most probably due to photodecomposition of the flavonoids [58-60]. This is consistent with the disappearance of the flavonoid IR bands and, in the case of 3HF-loaded NPs, with the appearance of small IR band(s) in the 1700-1760 cm^{-1} region (not shown), as expected for the photorearrangement product [60, 61].

Conditions	**Absorption bands**			
3HF in MeCN [29]	305 nm	341 nm	~352 nm	~410 nm (traces, anion)
3HF in MCM-41	315 nm	344 nm, broad		
3HF in MCM-41 aged sample	315 nm	342, broad		
7HF in MeCN	237 nm (sh)	250 nm	300 nm	
7HF in MCM-41		251 nm	311 nm	321 nm (sh) 368 (very weak sh)
7HF in MCM-41 aged sample		251 nm	312 nm	320 nm (sh) 368 (very weak sh)

Table 1. UV-Vis absorption bands observed for 3HF and 7 HF under different conditions.

The fluorescence spectra of flavonoid-loaded NPs suggest that the emitting species have different interactions with the surrounding environment as compared to the same molecules in solutions. This can easily be seen by the comparison of the emission spectrum of 3HF in MCM-41 with the one obtained in pure solvents. The main emission band of the fluorescence spectrum (λ_{exc} = 320 nm) of 3HF in MCM-41 is centred at 506 nm, a value much lower than what is observed in MeCN, but also in many other solvents, with only the significant exception of 2,2,2-trifluoroethanol [26]. This suggests that 3HF experiences a surrounding environment characterized by high hydrogen bonding donating (HBD) acidity, as it can be expected given the acidity of silanol groups and the high HBD capability of water molecules adsorbed on the silica surface. This is also confirmed by the presence of a relatively intense band at ~403 nm, typical of a N* emission (always present in hydrogen bonding donating environment [26]; this band is much weaker in MeCN solutions [32]). In the case of 3HF in MCM-41, stable and strong hydrogen bond interactions between the silanol and the OH and C=O groups of the flavonoid are likely to be formed. This is consistent with a previous study on quercetin in MCM-41 NPs, where the authors underlined the relevance of the hydrogen bonds interactions between silanols and quercetin [46].

The width of the blue-shifted 3HF emission band (extending to ~440 nm, see Figure 3) cannot exclude the presence of some fluorescence from a minor population of 3HF cation, whose emission is expected in the 420-450 nm region (see Table 3; see also [59]).

Excitation at 300 nm of 7HF-MCM-41 samples gives an emission peaking at 390 nm. In order to figure out the nature of the emitting species, fluorescence spectra for 7HF in different MeCN solutions (exposed to air, to mimic the conditions of 7HF in NPs) were recorded. When the fluorescence spectrum of 7HF in neutral MeCN is recorded (λ_{exc} = 300 nm) a weak band at 370 nm is observed, along with a weaker and broader band at ~530 nm (see Figure 4). Spectra recorded after some minutes of illumination show an increase of the intensity of the 370 nm band, strongly suggesting that this band can be ascribed to a photodecomposition product[1]. It cannot be excluded that a small contribution arises also from the neutral form of 7HF, given that the excitation spectrum recorded at 400 nm shows a maximum at 293 nm (i.e. very close to the absorption band of neutral 7HF). TD-DFT calculations also foresee an emission at 378 nm for the neutral form of 7HF. However this is at odds with previous results [25] where neutral 7HF in MeCN was reported to be non-fluorescent. Whereas this apparent discrepancy could be explained by the high sensitivity of our instrument (the fluorescence quantum yield value is 0.001), the most likely explanation is that the 370 nm emission is essentially given by a photodecomposition product.

[1] This is also in agreement with TLC analysis of a MeCN solution of 7HF after 30 minutes of illumination (not shown), showing indication of a photoproduct more polar than 7HF.

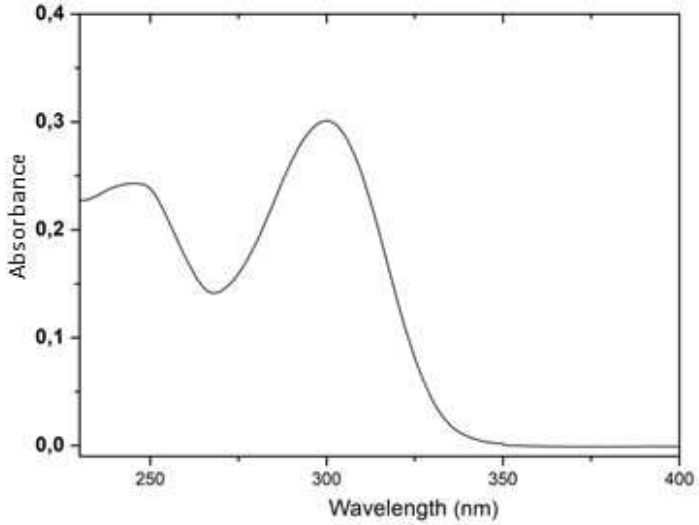
Absorbance
Wavelength (nm)

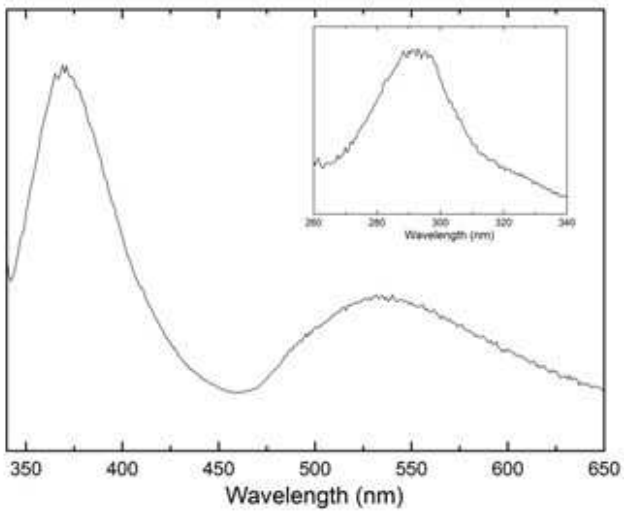
Wavelength (nm)

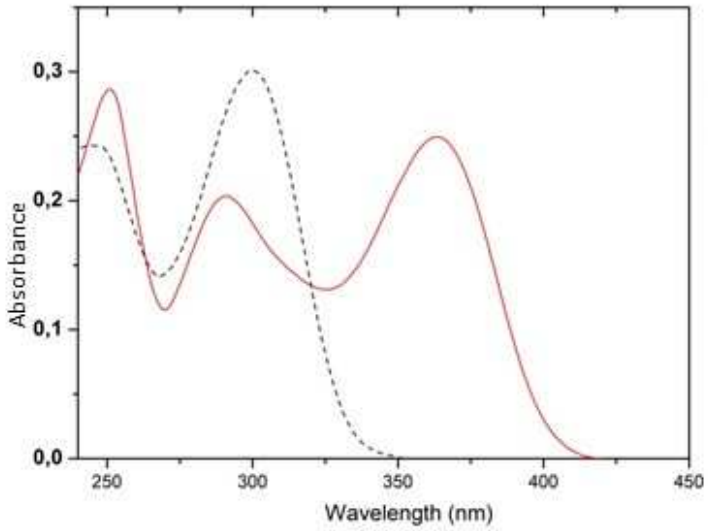
Absorbance
Wavelength (nm)

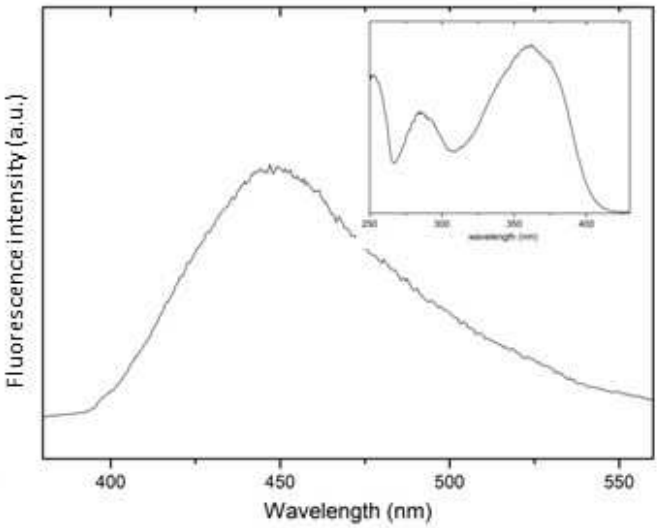
Fluorescence intensity (a.u.)
Wavelength (nm)

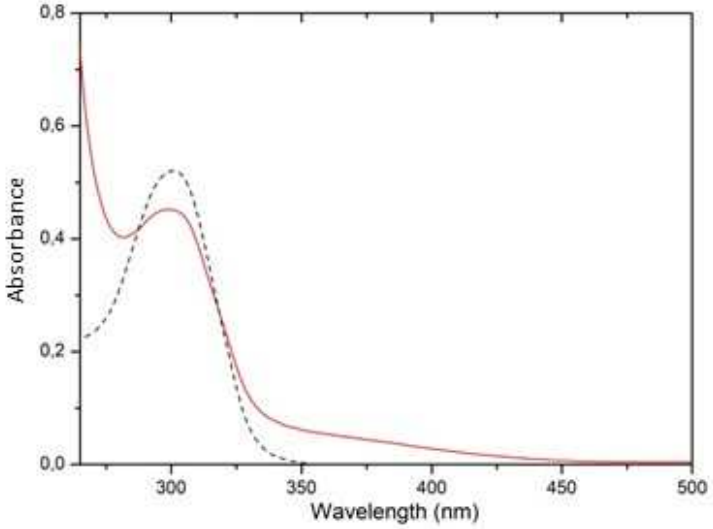
Absorbance
Wavelength (nm)

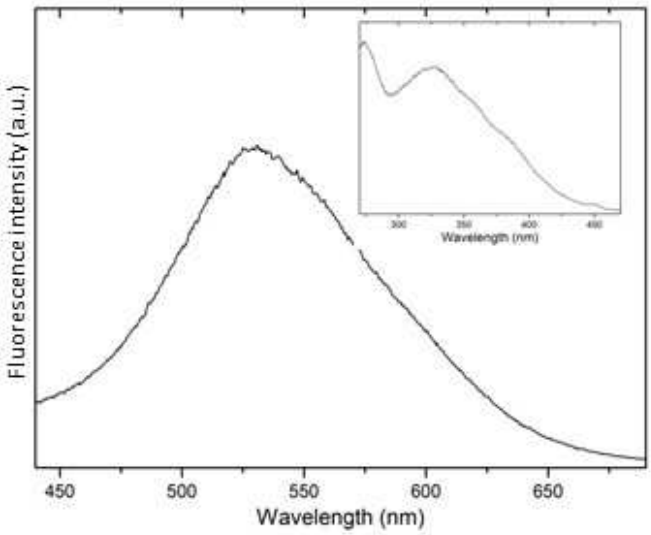
Fluorescence intensity (a.u.)
Wavelength (nm)

Figure 4. Upper panels: Left, UV-Vis absorption spectrum of 7HF in neutral MeCN. Right, Fluorescence spectrum of 7HF in neutral MeCN with λexc = 300 nm. Inset: fluorescence excitation spectra of 7HF in neutral MeCN, λem = 390 nm

Middle panels: Left, absorption spectra of 7HF in neat MeCN (black, dotted line) and in MeCN in the presence of 0.02 M H_2SO_4 (red). Right panel: Emission spectrum (λex = 300 nm) of 7HF in a 0.02 M H_2SO_4 solution in MeCN. Inset: excitation spectrum (λem = 449 nm) of 7HF in a 0.02 M H_2SO_4 solution in MeCN.

Lower panels: left, absorption spectra of 7HF in neat MeCN (black dotted line) and in MeCN in presence of Et_3N 0.05 M. Right: emission (black, λ_{ex}=370 nm) of 7HF in presence of Et_3N 0.05 M. Inset: excitation spectrum (red, λ_{em} = 529 nm) of 7HF in in MeCN in the presence of Et_3N 0.05 M

On the basis of these experiments, we have tried to understand the nature of the fluorescent form of 7HF in MCM-41. The huge increase of fluorescence weighs in against neutral 7HF: it is unlikely that the neutral form N would be responsible for such an intense emission. The fluorescence spectra recorded after some minutes of illumination (see [62]), on the other hand, suggests that the fluorescence is probably not due to a photodecomposition product (in such case, an increase of its intensity would be expected, as observed in MeCN solution).Fluorescence of the 7HF anion is expected to be at $\lambda > 520$ nm (see Figure 4 and TD-DFT results in Table 3; see also [25]) and therefore is not compatible with the observed fluorescence at 390 nm. Furthermore, despite the presence of MeCN molecules in the NPs, it is unlikely that they would be able to reproduce conditions observed in MeCN solutions, given the presence of adsorbed water molecules and acidic Si-OH groups on the silica surface. Such an acidic environment could suggest partial formation of a cationic form of 7HF through a silanol-to-carbonyl proton transfer. Indeed, the fluorescence excitation spectrum of 7HF in MCM-41 has a maximum at 337 nm. Interestingly, this excitation wavelength is in rough agreement with the one observed for 7HF cation **C** in MeOH/H_2O (λ = 366 nm) [25]. The fluorescence of the cation of MeOH is observed at much longer wavelength (λ_{em} = 464 nm) but it has been shown that the position of the emission band depends on the acidity of the surrounding medium [25, 63]. To get more precise information on this point, we have carried out 7HF absorption and fluorescence studied in MeCN in presence of H_2SO_4 (concentration 0.02 M) and performed some TD-DFT calculations to reproduced the experimental spectra. In acidified MeCN an absorption maximum is observed at 363 nm (see Figure 4), in good agreement with the maximum of the fluorescence excitation spectrum (361 nm). TD-DFT calculations (Table 3) foresee a UV-Vis absorption maximum at 370 nm. The experimental fluorescence maximum (λ_{exc} = 300 nm) is observed at 448 nm, in good agreement with the calculated TD-DFT values of 453 nm (for the conformer "cation2" with the OH of the protonated carbonyl pointing towards the hydrogen in position 3; see Figure S4 in ESI) and of 421 nm (for the conformer "cation1" with the OH pointing in the opposite direction). However, following the discussion in [25], in such conditions phototautomer formation can take place. Our TD-DFT calculation foresee a fluorescence emission for the tautomer in the 594-610 nm range, which seems too far from the observed 448 nm emission peak. However, it is not excluded that the phototautomer contributes at least to he red-shifted tail of the fluorescence band, which extends beyond 550 nm (see Figure 3).

This may help to clarify the real identity of the emitting species in 7HF-doped NPs, because its emission maximum is at 390 nm (with a long tail extending beyond 550 nm) when the excitation wavelength is 300 nm. Whereas there is no clear evidence that the environment around 7HF (cation) inside MCM-41 pores can be properly simulated by the dielectric constant of MeCN (such assumption was based on the presence of several MeCN molecules per flavonoid molecule inside the NP, and on the polarity of the internal silica surfaces), no speculation can be made on specific 7HF-surface interactions (e.g. hydrogen bonds) and/or on peculiar conformations adopted by 7HF inside the pores of the NP. It is however significant to notice that

previous DFT calculations have shown that specific solute-solvent interactions may significantly affect the energetics and electronic structure of 7HF [25]. Furthermore, our TD-DFT calculations foresee a 32 nm shift in the emission wavelength by simply changing the orientation of the OH of the protonated carbonyl, suggesting that any surface-induced peculiar conformation of 7HF cation may entail a change from the behaviour observed in solution, i.e. an isotropic environment. However, as mentioned above, according to [25], in acidic conditions phototautomer can be formed from the cation. This suggests that the emitting species could be the phototautomer originating from the cationic form of 7HF. The position of the emitting band is far (~200 nm) from what is foreseen by TD-DFT calculation for the tautomer in MeCN, but it should be underlined that these calculations are probably not appropriate to simulate the fluorescence of a phototautomer formed from a cation adsorbed on a hydrated silica surface.

Finally, it is important to underline that the observed UV-Vis spectrum of 7HF-doped NPs shows a maximum at 311 nm and a shoulder at ~321 nm, with a weak shoulder at 368 nm. This suggests that several sub-populations of 7HF exist in MCM-41 NPs, the most fluorescent being probably of cationic or phototautomeric (originating from 7HF cation) forms. The presence of the 311 nm band however suggests that a large fraction of 7HF molecules exist in neutral state.

Time-resolved emission analysis show that both flavonoids have a longer fluorescence lifetime inside NPs compared to solutions (see Figure 5). This outcome is not unexpected: in silica NPs, flavonoid rotation is most probably strongly restricted, and this could reduce the non-radiative dissipation of the excitation energy, leading to and increase of fluorescence lifetime.

The presence of three different lifetime constants in the in both 3HF- and 7HF- loaded NPs suggests that in both cases three subpopulations of flavonoids are present. For 7HF NPs this observation is in agreement with the presence of three absorption bands at 311, 321, and 368 nm.

	Blue-shifted emission (nm)	Red-shifted emission (nm)	Overall quantum yield	Excitation spectrum (nm)
3HF in MeCN	395 (very weak)	526	0.081	305, 340 (λ_{em} = 600)
3HF in MCM-41 fresh sample	403 (broad) (λ_{exc} = 320)	506 (λ_{exc} = 320)	0.078	349, 362 (λ_{em} = 575)
3HF in MCM-41 aged sample	403 broad (λ_{exc} = 320)	506 (λ_{exc} = 320)	0.068	348 (shoulder), 364; 427 (weak, broad) (λ_{em} = 575)
7HF in MeCN	372 weak; 530 very weak, broad (λ_{exc} = 300)		0.001	293 (λ_{em} = 400)
7HF anion (7HF + TEA) in MeCN	533 (weak) (λ_{exc} = 300); 529 (λ_{exc} = 375)		-	325; 352 sh; 377 sh (λ_{em} = 529)
7HF anion (7HF + DBU) in MeCN	583 (λ_{exc} = 350)		-	
7HF cation (7HF+ 0.02 M H_2SO_4 in MeCN)	447 (λ_{exc} = 300)		-	360, 372 sh (λ_{em} = 449)
7HF MCM-41	390 (λ_{exc} = 300)		0.033	337, 390 (very weak) (λ_{em} = 550)
7HF in MCM-41 aged sample	394 (λ_{exc} = 300)		0.036	338, 428 (λ_{em} = 550)

Table 2. Fluorescence properties of 3HF and 7HF in different systems under different conditions.

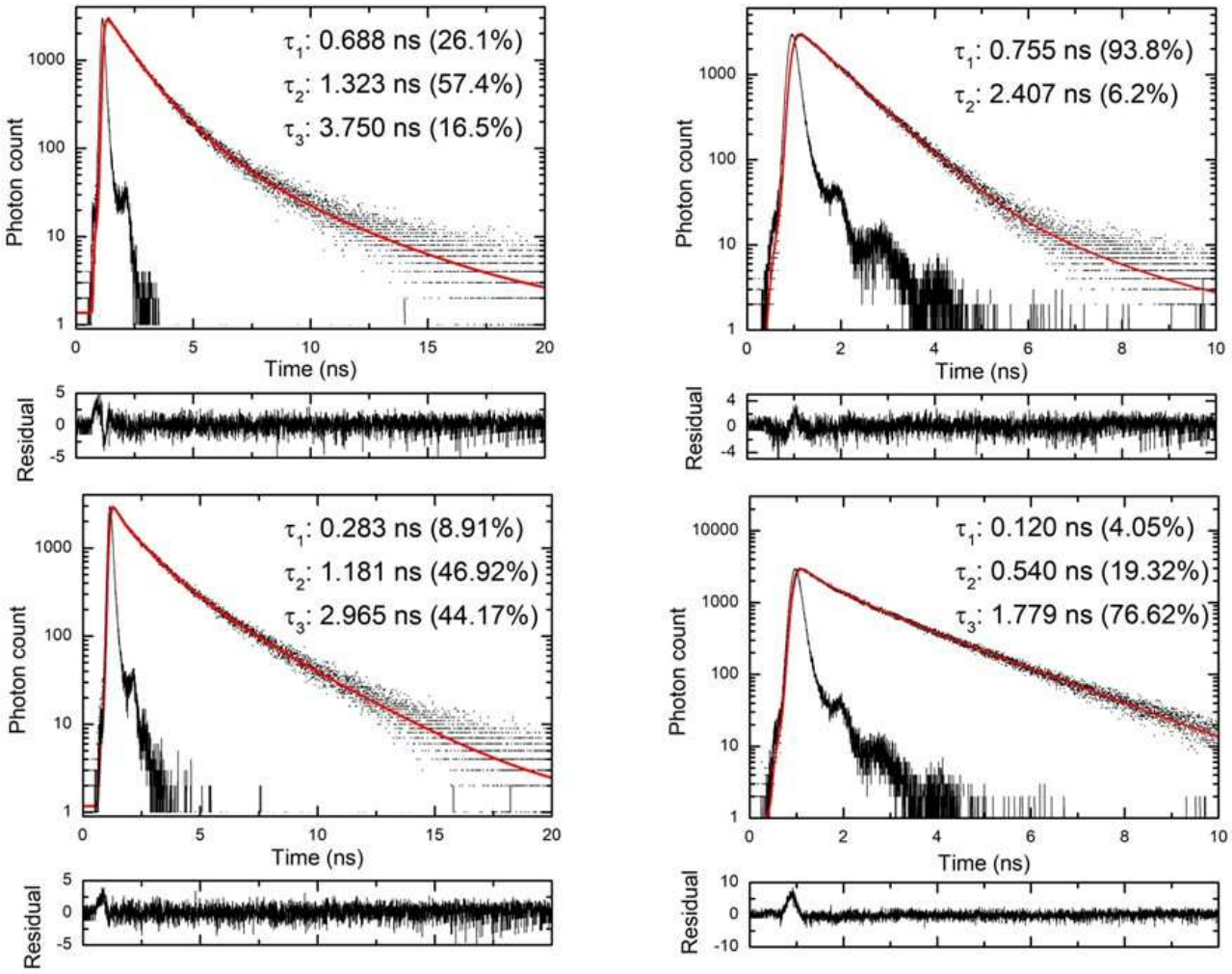

Figure 5. Time-resolved fluorescence of 3HF-doped NPs (upper panel, left; λ_{exc} = 372 nm; λ_{em} = 500 nm). Time resolved fluorescence of 3HF in MeCN (upper panel, right; λ_{exc} = 372 nm; λ_{em} = 530 nm). Time-resolved fluorescence of 7HF-doped NPs (lower panel, left; λ_{exc} = 372 nm; λ_{em} = 420 nm), 7HF in MeCN (lower panel, right; λ_{exc} = 372 nm; λ_{em} = 540 nm)

Both flavonoid-loaded NPs shows a decrease in photoluminescence after prolonged illumination (see Figure 6 and fluorescence spectra in [62]), but without significant modification in the emission spectrum. It is interesting to compare this result to the photostability of the flavonoids in MeCN solutions. Both 3HF and 7HF look more stable inside NPs, suggesting a role of the silica matrix in preserving the fluorophore (see Figure 6). Interestingly, both 3HF-doped and 7HF-doped NPs remain fluorescent after two months of exposure to air at room temperature, with roughly the same quantum yield (see Table 2).

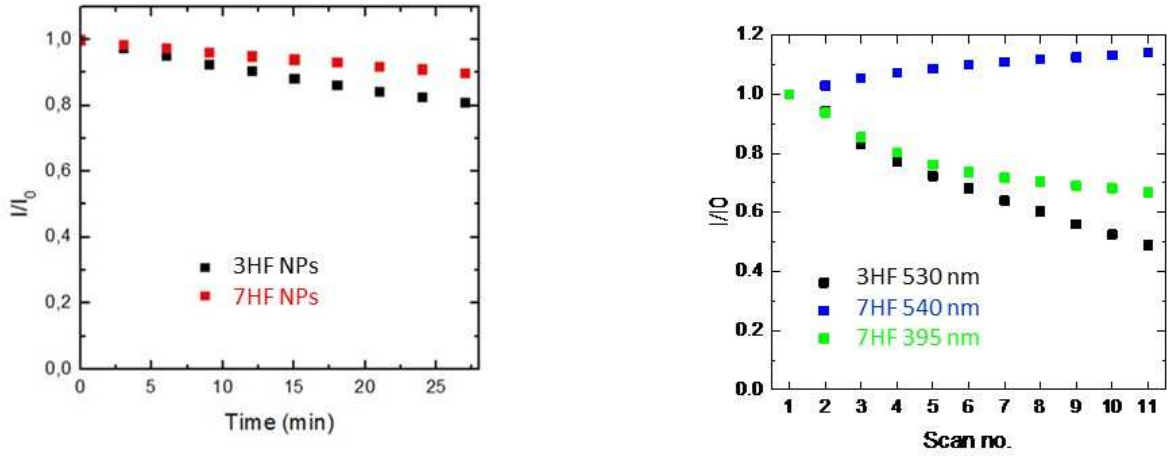

Figure 6. Left panel: Kinetics of decrease of fluorescence intensity recorded every 3 minutes during continuous exposure to UV-light of 3HF-doped NPs (upper left panel; λ_{exc} = 320 nm) and 7HF-dopep NPs (upper right panel λ_{exc} = 300 nm). Right panel: kinetics of fluorescence intensity for 3HF and 7HF in MeCN solution. For 7HF the 540 nm band diminishes its intensity, whereas it grows for the 395 nm. This strongly suggests that the 395 nm is – at least partially – due to a photodecomposition product. Entire fluorescence spectra after increasing illumination times are reported in [62].

	Absorbance	Fluorescence
3HF neutral		
free/gas phase	3.552 eV 349.1 nm	3.128 eV 396.4 nm
MeCN	3.496 eV 354.7 nm	2.908 eV 426.4 nm
3HF tautomer		
free/gas phase	2.572 eV 482.1 nm	2.295 eV 540.3 nm
MeCN	2.607 eV 475.7 nm	2.182 eV 568.1 nm
3HF anion		
free/gas phase	2.335 eV 531.0 nm	2.029 eV 611.2 nm
MeCN	2.597 eV 477.4 nm	2.184 eV 567.6 nm
3HF cation 1		
free/gas phase	3.126 eV 396.7 nm	2.390 eV 518.8 nm
MeCN	3.172 eV 390.9 nm	2.756 eV 449.9 nm
3HF cation 2		
free/gas phase	3.345 eV 370.7 nm	2.823 eV 439.2 nm
MeCN	3.331 eV 372.2 nm	2.818 eV 440.0 nm
7HF neutral		
free/gas phase	3.532 eV 351.0 nm	2.845 eV 435.8 nm
MeCN	3.780 eV 328.0 nm	3.281 eV 377.9 nm
7HF tautomer 1		
free/gas phase	2.655 eV 467.0 nm	1.734 eV 713.0 nm
MeCN	2.855 eV 434.3 nm	2.086 eV 594.4 nm
7HF tautomer 2		
free/gas phase	2.590 eV 478.7 nm	1.680 eV 738.1 nm
MeCN	2.742 eV 452.2 nm	2.033 eV 609.9 nm
7HF anion		
free/gas phase	2.049 eV 605.0 nm	1.496 eV 828.8 nm
MeCN	2.891 eV 428.9 nm	2.194 eV 565.2 nm
7HF cation 1		
free/gas phase	3.352 eV 369.9 nm	3.003 eV 412.9 nm
MeCN	3.350 eV 370.1 nm	2.943 eV 421.3 nm
7HF cation 2		
free/gas phase	3.330 eV 372.4 nm	2.736 eV 453.2 nm
MeCN	3.338 eV 371.4 nm	2.894 eV 428.4 nm

Table 3. Calculated absorption and emission spectra for the different species. For the absorption spectra, only the more red-shifted band is indicated. The comparison between gas phase and solvated (MeCN) molecules gives an estimation of the influence of the surrounding environment. See [62] for more detailed data.

Conclusions

In this work, we have prepared 3HF and 7HF doped silica MCM-41 NPs by a simple post-doping procedure. Both kinds of NPs have proved to be highly fluorescent, their emission properties being little affected by ageing and only moderately by UV exposure. For 3HF, interestingly, despite its overall hydrophobic character and the capability of donating and accepting hydrogen bonds of the 3OH group and the hydrogen bond basicity of its C=O moiety, the photophysics is strikingly similar to the one observed in solution. For 7HF, the emitting species is probably the cationic and/or the phototautomeric form.

Such results show a simple and efficient way of encapsulating the two flavonoids in silica NPs, keeping their fluorescence properties. On the other hand, it provides some initial information on the interactions between 3HF and 7HF with silica surfaces. Spectroscopic data also suggest that both flavonoids form strong hydrogen bond interactions with silanol groups and adsorbed water molecules; at least in the case of 7HF, a surface-to-flavonoid proton transfer seems to take place in a significant fraction of flavonoid molecules.

References

[1] Agati G, Tattini M. Multiple functional roles of flavonoids in photoprotection. New Phytologist 2010; 186: 786-793. doi:10.1111/j.1469-8137.2010.03269.x

[2] Agati G, Azzarello E, Pollastri S, Tattini M. Flavonoids as antioxidants in plants: Location and functional significance. Plant Sci. 2012; 196: 67-76. doi:10.1016/j.plantsci.2012.07.014

[3] Buer CS, Imin N, Djordjevic MA, Flavonoids: New Roles for Old Molecules. J. Integr. Plant Biol 2010; 52: 98-111. doi:10.1111/j.1744-7909.2010.00905.x

[4] Havsteen B. The Biochemistry and Medical Significance of the Flavonoids. Pharmacol. Ter. 2002; 96: 67-202. doi:10.1016/S0163-7258(02)00298-X

[5] Rodriguez-Mateos A, Vauzour D, Krueger CG, Shanmuganayagam D, Reed J, Calani L, Mena P, Del Rio D, Crozier A. Bioavailability, Bioactivity and Impact on Health of Dietary Flavonoids and Related Compounds: An Update. Arch. Toxicol. 2014; 88: 1803-1853 doi:10.1007/s00204-014-1330-7

[6] Borges Bubols G, da Rocha Vianna D, Medina-Remon A, von Poser G, Lamuela-Raventos, RM.; Eifler-Lima, VL, Garcia SC. The antioxidant activity of coumarins and flavonoids. Mini Rev. Med. Chem. 2013; 13: 318-334. doi:10.2174/138955713804999775

[7] Jovanovic SL, Steenken S, Tosic M, Marjanovic B, Simic MG. Flavonoids as antioxidants. J. Am. Chem. Soc. 1994; 116: 4846-51. doi:10.1021/ja00090a032

[8] Burda S, Oleszek W. Antioxidant and antiradical activities of flavonoids. J. Agr. Food. Chem. 2001; 49: 2774-79 doi:10.1021/jf001413m

[9] Musialik M, Kuzmicz R, Pawlowski TS, Litwinienko G. Acidity of Hydroxyl Groups: An Overlooked Influence on Antiradical Properties of Flavonoids. J. Org. Chem 2009; 74: 2699-2709. doi:10.1021/jo802716v

[10] Youdim KA, Shukitt-Hale B, Joseph JA. Flavonoids and the brain: interactons at the blood-brain barrier and their physiological effects on the central nervous system. Free Radic. Biol. Med. 2004; 37: 1683-1693. doi:10.1016/j.freeradbiomed.2004.08.002

[11] Solanki I, Parihar P, Mansuri ML, Parihar MS Flavonoid-based therapies in the early management of neurodegenerative diseases. Adv. Nutr. 2015; 6: 64-72. doi:10.3945/an.114.007500

[12] Zhao J, Zhu M, Kumar M, Ngo FY, Li Y, Lao L, Rong J.
A Pharmacological Appraisal of Neuroprotective and Neurorestorative Flavonoids Against Neurodegenerative Diseases. CNS Neurol Disord Drug Targets 2019;18:103-114.
doi:10.2174/1871527317666181105093834

[13] Kopustinskiene DM, Jakstas V, Savickas A, Bernatoniene. Flavonoids as anticancer agents. J. Nutrients. 2020; 12: 457 doi: 10.3390/nu12020457

[14] Rodriguez-Garcia C, Sanchez-Quesada C, Gaforio JJ. Dietary Flavonoids as Cancer Chemopreventive Agents: An Updated Review of Human Studies. Antioxidants 2019; 8: 137
doi:10.3390/antiox8050137

[15] Raffa D, Maggio B, Raimondi MV, Plescia F, Daidone G, Recent Discoveries of Anticancer Flavonoids. Eur J Med. Chem. 2017; 142: 213-228
doi: 10.1016/j.ejmech.2017.07.034

- [16] Pyrzynska K, Pekal A, Flavonoids as analytical reagents. Crit. Rev. Anal. Chem. 2011; 41: 335-345**.**
doi :10.1080/10408347.2011.607077

[17] Kathyal M, Prakash S, Analytical reactions of hydroxyflavones. Talanta 1977; 24: 367-375.
doi:10.1016/0039-9140(77)80022-2

[18] Das S, Rohman MA, Singha Roy A. Exploring the Non-Covalent Binding Behaviours of 7-hydroxyflavone and 3-hydroxyflavone With Hen Egg White Lysozyme: Multi-spectroscopic and Molecular Docking Perspectives. J. Photochem. Photobiol. B. 2018; 180:25-38 . doi: 10.1016/j.jphotobiol.2018.01.021

[19] Sengupta B, Sahihi M, Dehkhodaei M, Kelly D, Arany I. Differential roles of 3-Hydroxyflavone and 7-Hydroxyflavone against nicotine-induced oxidative stress in rat renal proximal tubule cells. PLoS One. 2017; 12(6):e0179777 doi: 10.1371/journal.pone.0179777

[20] Sengupta B, Reilly SM, Davis DE Jr, Harris K, Wadkins RM, Ward D, Gholar D, Hampton C. Excited State Proton Transfer of Natural Flavonoids and Their Chromophores in Duplex and Tetraplex DNAs. J. Phys. Chem. B. 2015; 119:2546-56. doi: 10.1021/jp508599h.

[21] Montana P, Pappano N, Debattista N, Avila V, Posadaz A, Bertolotti SG, Garcia NA.The activity of 3- and 7-hydroxyflavones as scavengers of superoxide radical anion generated from photo-excited riboflavin. Can. J. Chem. 2003 81: 909-914
doi: 10.1139/v03-097

[22] Lu KH, Chen PN, Hsieh YH, Lin CY, Cheng FY, Chiu PC, Chu SC, Hsieh YS. 3-Hydroxyflavone Inhibits Human Osteosarcoma U2OS and 143B Cells Metastasis by Affecting EMT and Repressing u-PA/MMP-2 via FAK-Src to MEK/ERK and RhoA/MLC2 Pathways and Reduces 143B Tumor Growth in Vivo. Food Chem. Toxicol. 2016;97:177-186. doi: 10.1016/j.fct.2016.09.006

[23] Lau AJ, Chang TK. 3-Hydroxyflavone and Structural Analogues Differentially Activate Pregnane X Receptor: Implication for Inflammatory Bowel Disease. Pharmacol. Res. 2015; 100: 64-72. doi: 10.1016/j.phrs.2015.07.031

[24] Wang J, Su H, Zhang T, Du J, Cui S, Yang F, Jin Q. Inhibition of Enterovirus 71 Replication by 7-Hydroxyflavone and Diisopropyl-Flavon7-yl Phosphate. PLoS One. 2014;9:e92565.

doi: 10.1371/journal.pone.0092565

[25] Serdiuk IE, Varenikov AS, Roshal AD. 7-hydroxyflavone Revisited: Spectral, Acid-Base Properties, And Interplay of the Protolytic Forms in the Ground and Excited States. J. Phys. Chem. A 2014, 118, 3068-3080. doi: 10.1021/jp412334x

[26] Lazzaroni S, Dondi D, Mezzetti A, Protti S, Role of Solute-Solvent Hydrogen Bonds on the Ground State and the Excited State Proton Transfer in 3-hydroxyflavone. A Systematic Spectrophotometric Study. Photochem. Photobiol. Sci. 2018; 17(7):923-933. doi: 10.1039/c8pp00053k.

[27] Protti S, Mezzetti A. Any colour you like. Excited state and ground state proton transfer in flavonols and applications. Albini A. (Ed) Specialistic Periodical Report: Photochemistry, Royal Society of Chemistry, 2012; 40: pp 295–322. doi: 10.1039/9781849734882-00295

[28] Mezzetti A, Protti S. Flavonols and 3-hydroxychromones: new applications for a class of environment-sensitive fluorescent molecules. Chimica Oggi – Chem. Today 2020, 38, 34-37

[29] Zhu K, Lv T, Qin T, Huang Y, Wang L, Liu B. A flavonoid-based fluorescent probe enables the accurate quantification of human serum albumin by minimizing the interference from blood lipids. Chem. Comm. 2019, 55, 13983-86. DOI: 10.1039/c9cc08015e

[30] Liu B, Bi X, McDonald L, Pang Y, Liu D, Pan C, Wang L, Solvatochromic fluorescent probes for recognition of human serum albumin in aqueous solution: Insights into structure-property relationship. Sens. Act. B. Chem 2016, 236, 668-674. https://doi.org/10.1016/j.snb.2016.06.056

[31] Qin T , Liu B, Huang Y , Yang K, Zhu K, Luo Z, Pan C , Wang L. Ratiometric fluorescent monitoring of methanol in biodiesel by using an ESIPT-based flavonoid probe. Sens Act. B. Chem 2018, 277, 484-491. https://doi.org/10.1016/j.snb.2018.09.056

[32] Loco D, Protti S, Mennucci B, Mezzetti A. Critical assessment of solvent effects on absorption and fluorescence of 3HF in acetonitrile in the QM/PCM framework: A synergic computational and experimental study. J. Mol. Struct. 2019; 1182: 283-291. doi: 10.1016/j.molstruc.2018.12.085

[33] Chaudhuri S, Pahari B, Sengupta PK. Ground and Excited State Proton Transfer and Antioxidant Activity of 7-hydroxyflavone in Model Membranes: Absorption and Fluorescence Spectroscopic Studies. Biophys. Chem. 2009; 139:29-36.
doi: 10.1016/j.bpc.2008.09.018

[34] Carturan S, Quaranta A, Maggioni G, Bonafini M, Della Mea G. 3-Hydroxyflavone-based wavelength shifting systems for near UV optical sensors. Sensors and Actuators A: Physical 2004 ; 113 : 288-292. doi:10.1016/j.sna.2004.01.048

[35] Protti S, Raulin K, Cristini O, Kinowski C, Turrell S, Mezzetti A, Wavelength shifting systems based on flavonols and their metal complexes encapsulated by post-doping in porous SiO_2 xerogel matrices. J. Mol. Struct. 2011; 993, 485-490. doi:10.1016/j.molstruc.2011.02.010

[36] Maciejewicz W, Soczewinski E. Chemometric characterization of TLC systems of the type silica-binary non-aqueous mobile phase in the analysis of flavonoids. Chromatographia 2000; 51: 473–477. doi:10.1007/BF02490487

[37] de Rijke E, Out P, Niessen WM, Ariese F,Gooijer C, Brinkman UA. Analytical separation and detection methods for flavonoids. J. Chromat. A 2006; 1112:31-63 doi: 10.1016/j.chroma.2006.01.019

[38] Lungare S, Hallam K, Badhan RKS, Phytochemical-loaded Mesoporous Silica Nanoparticles for Nose-To-Brain Olfactory Drug Delivery. Int. J. Pharm. 2016; 513: 280-293. doi: 10.1016/j.ijpharm.2016.09.042.

[39] Arriagada F, Gunther G, Morales J, Nanoantioxidant–Based Silica Particles as Flavonoid Carrier for Drug Delivery Applications Pharmaceutics 2020; 12: 302. doi:10.3390/pharmaceutics12040302

[40] Brezoiu A-M., Matei C, Deaconu M, Stanciuc A-M., Trifan A, Gaspar-Pintiliescu A, Berger D, Polyphenols extract from grape pomace. Characterization and valorisation through encapsulation into mesoporous silica-type matrices Food Chem. Toxic. 2019; 133: 110787 doi: 10.1016/j.fct.2019.110787

[41] Arriagada F , Correa O, Gunther G, Nonell S, Mura F, Olea-Azar C, Morales J. Morin Flavonoid Adsorbed on Mesoporous Silica, a Novel Antioxidant Nanomaterial. PLOS One 2016; 11: e0164507, doi: 10.1371/journal.pone.0164507

[42] Das S, Batuta S, Alam Md N, Fouzder C, Kundu R, Mandal D, Begum NA, Antioxidant flavone analog functionalized fluorescent silica nanoparticles: Synthesis and Exploration of their possible use as a biomolecule sensor. Coll. Surf. B. – Biointerf. 2017; 157: 286-296. doi: 10.1016/ j.colsurfb.2017.05.074

[43] Ferreira G, Hernandez-Martinez AR, Pool H, Molina G, Cruz-Soto M; Luna-Barcenas G, Estevez M, Synthesis and functionalization of silica-based nanoparticles with fluorescent biocompounds extracted from Eysenhardtia polystachya for biological application. Mat. Sci. Eng. C-Mater. 2015; 57: 49-57. doi:10.1016/j.msec.2015.07.012

[44] Karpov SI, Korabel'nikova EO, Separation of (+)-catechin and quercetin on mesoporous MCM-41 composites: dynamics of the sorption of flavonoids. Russian J. Phys. Chem. A 2015; 89: 1096-1102 doi:10.1134/S0036024415060151

[45] Wang XY, Li J, Yang XJ, Gao XM, Wang H, Chang YX, A rapid and efficient extraction method based on industrial MCM-41-miniaturized matrix solid-phase dispersion extraction with response methodology for simultaneous quantification of six flavonoids in *Pollen typhae* by ultra-high-performance liquid chromatography J. Sep. Sci. 2019; 42: 2426-2434. doi:10.1002/jssc.201900227

[46] Berlier G, Gastaldi L, Ugazio E, Miletto I, Iliade P, Sapino S. Stabilization of quercetin flavonoid in MCM-41 mesoporous silica: Positive effect of surface functionalization. J. Coll. Interf. Sci. 2013, 393, 109-118. doi: 10.1016/j.jcis.2012.10.073

[47] Berlier G, Gstaldi L, Sapino S, Miletto I, Bottinelli E, Chirio D, Ugazio E, ; MCM-41 as a useful vector for rutin topical formulations: synthesis, characterization and testing Int J. Pharm. 2013, 457, 177-186. doi: 10.1016/j.ijpharm.2013.09.018

[48] Meynen V, Cool P, Vansant EF. Verified syntheses of mesoporous materials, Microporous and Mesoporous Materials 2019;125: 170–223. doi:10.1016/j.micromeso.2009.03.046

[49] Hohenberg P, Kohn W. Inhomogenous electron gas. Phys. Rev. B 1964; 136: 864-871.

doi: 10.1103/PhysRev.136.B864

[50] Runge E, Gross EKU. Density-functional theory for time-dependent systems. Phys. Rev. Lett. 1984; 52: 997-1000. doi: 10.1103/PhysRevLett.52.997

[51] Kim K, Jordan KD. Comparison of density functional and MP2 calculations on the water monomer and dimer. J. Phys. Chem. 1994; 98: 10089–10094. doi: 10.1021/j100091a024

[52] Barone V, Cossi M. Quantum calculation of molecular energies and energy gradients in solution by a conductor solvent model. J. Phys. Chem. A 1998; 102: 1995–2001.
doi: 10.1021/jp9716997

[53] Neese F. Software update: the ORCA program system, version 4.0 (WIREs Comput Mol Sci 2018, 8:e1327. doi: 10.1002/wcms.1327)

[54] M. J. Frisch et alia, Gaussian, Inc., Wallingford CT, 2009

[55] Wang M, Teslova T, Xu F, Spataru T, Lombardi JR, Birke RL, Leona M, Raman and Surface Enhanced Raman Scattering of 3-Hydroxyflavone J. Phys. Chem. C 2007; 111: 3038–3043
https://doi.org/10.1021/jp062100i

[56] Tyukavkina NA, Pogodaeva, NN, Ultraviolet absorption of flavonoids II. Ionization constants of 7- and 4′-hydroxy derivatives of flavone and flavonol. Chem. Nat. Compd. 1971 ; **7 :** 8–11.
https://doi.org/10.1007/BF01032014

[57] Seitsonen AP, Idrissi A, Protti S, Mezzetti A, Solvent effects on the vibrational spectrum of 3-hydroxyflavone, J. Mol. Liq. 2019, 275, 723-728. https://doi.org/10.1016/j.molliq.2018.11.020

[58] Protti S, Mezzetti A, Solvent effects on the photophysics and photoreactivity of 3-hydroxyflavone: A combined spectroscopic and kinetic study. J. Mol. Liq. 2015; 205: 110-114.
doi:10.1016/j.molliq.2014.12.001

[59] Schipfer R, Wolfbeis OS, Knierzinger A, pH-Dependent fluorescence spectroscopy. Part 12. Flavone, 7-hydroxyflavone, and 7-methoxyflavone. J. Chem. Soc., Perkin Trans. 2 1981; 1443-1448.
doi:10.1039/P29810001443

[60] Protti S, Mezzetti A, Lapouge C, Cornard J-P. Photochemistry of metal complexes of 3-hydroxyflavone: towards a better understanding of the influence of solar light on the metal–soil organic matter interactions. Photochem. Phoobiol. Sci 2008; 7, 109-119. doi: 10.1039/b709682h

[61] Tomar J, Kaur K, Bansal M, The detection of the precursors of the photorearranged products of 3-hydroxyflavones in selected solvents from UV-visible spectra *in situ*. Photochem. Photobiol. Sci. 2019 ;18 : 2912-2920. doi: 10.1039/C9PP00316A

[62] Landström A, Seitsonen AP, Leccese S, Abadian H, Lambert J-F, Concina I, Protti S, Mezzetti A, Data-in-Brief, submitted.

[63] Wolfbeis OS, Knierzinger A, Schipfer R. pH-dependent fluorescence spectroscopy XVII: First excited singlet state dissociation constants, phototautomerism and dual fluorescence of flavonol. J. Photochem. 1983; 21: 67-79. doi: 10.1016/0047-2670(83)80009-4